Evaluation of macrozone dimensions by ultrasound and EBSD techniques

Moreau, André; Toubal, Lotfi; Bocher, Philippe; Humbert, Michel; Uta, Elena; Gey, Nathalie

Publisher's version / Version de l'éditeur:
https://doi.org/10.1016/j.matchar.2012.09.011
Materials Characterization, 75, pp. 115-128, 2012-10-01

Evaluation of macrozone dimensions by ultrasound and EBSD techniques

André Moreau[1], Lotfi Toubal[1,2,3], Philippe Bocher[2], Michel Humbert[4], Elena Uta[4], Nathalie Gey[4]

1. National Research Council of Canada, 75 de Mortagne Blvd. Boucherville, QC, Canada J4B 6Y4.
2. Ecole de technologie supérieure, 1100, rue Notre-Dame Ouest, Montréal, QC, Canada H3C 1K3.
3. Present address: Université du Québec à Trois-Rivières, 3351, boul. des Forges, C.P. 500, Trois-Rivières, QC, Canada G9A 5H7.
4. Laboratoire d'Etude des Microstructures et de Mécanique des Matériaux (LEM3), UMR CNRS 7239, Université de Lorraine - Île du Saulcy - 57045 METZ Cedex 1 – France.

Corresponding author: André Moreau. Tel. 1-450-641-5237. Fax: 1-450-641-5106

e-mail: Andre.Moreau@cnrc-nrc.gc.ca

Abstract

Titanium alloys are known to have texture heterogeneities, i.e. regions much larger than the grain dimensions, where the local orientation distribution of the grains differs from one region to the next. The electron backscattering diffraction (EBSD) technique is the method of choice to characterize these macro regions, which are called macrozones. Qualitatively, the images obtained by EBSD show that these macrozones may be larger or smaller, elongated or equiaxed. However, often no well-defined boundaries are observed between the macrozones and it is very hard to obtain objective and quantitative estimates of the macrozone dimensions from these data. In the present work, we present a novel, non-destructive ultrasonic technique that provides objective and quantitative characteristic dimensions of the macrozones. The obtained dimensions are based on the spatial autocorrelation function of fluctuations in the sound velocity. Thus, a pragmatic definition of macrozone dimensions naturally arises from the ultrasonic measurement. This paper has three objectives: 1) to disclose the novel, non-destructive ultrasonic technique to measure macrozone dimensions, 2) to propose a quantitative and objective definition of macrozone dimensions adapted to and arising from the ultrasonic measurement, and which is also applicable to the orientation data obtained by EBSD, and 3) to compare the macrozone dimensions

obtained using the two techniques on two samples of the near-alpha titanium alloy IMI834. In addition, it was observed that macrozones may present a semi-periodical arrangement.

Keywords: macrozone, ultrasound, titanium, EBSD, texture, correlation

1. Introduction

1.1 Macrozones and texture heterogeneities

Macrozones are local texture heterogeneities found in forged titanium parts. These relatively large regions, sometimes of millimetric dimensions, have been detected using x-ray diffraction [1], texture-sensitive etching and optical metallography [2], and electron backscattering diffraction (EBSD) [3]. Some studies were focused on better understanding their origin [4-6] because macrozones are suspected to contribute to early fatigue damage of Titanium parts [7-8]. In fact, the mechanical properties of Titanium are strongly influenced by the texture. More precisely the c-axis orientation of the hexagonal close packed cell with respect to the stress is an important parameter that in most cases defines the activated slip systems and the crack nucleation mechanisms [9]. Especially, cold dwell fatigue cracks have been observed to nucleate by quasi-cleavage on α grains having their c-axes close to the tensile direction. Moreover, macrozones with a high fraction of α grains with c-axes close to the tensile direction have been identified as damage accumulation sites that can lead to premature failure of manufactured components.

To better understand the relationship between macrozones and mechanical properties, we need to obtain reliable quantitative information about them. Ultrasound velocity in hexagonal materials depends on the orientation of the c-axis and is potentially a good probe of macrozones in titanium. In a previous paper [10], it was shown that a sample with qualitatively coarser texture heterogeneities, as measured by ultrasonics, had different dwell-fatigue properties from 5 others. However, it would be desirable to obtain quantitative estimates of texture heterogeneities and macrozones characteristics such as size, orientation, and shape. This may allow determining more precisely the relationship between macrozone characteristics and the dwell-fatigue properties.

Approaches to estimating the size of texture heterogeneities were proposed only recently. For example, Wright et al. define two scalar measures of heterogeneity, "... one parameter for characterizing the severity of texture gradients and the other for quantifying the degree of texture banding" [11]. These parameters are based on calculating first and second derivatives of the mean angular deviation of a crystal direction from the sample normal (or any other reference direction) as a function of position in some spatial direction (such as the thickness direction). The parameters are simple and easy to interpret, but are limited in their potential range of applications. In contrast, Gao et al. propose a fully general treatment by calculating the two-point, or pair, correlation function of the orientation using a large set of metallographic planes [12]. The disadvantages of the later approach are its complexity and the difficulty to obtain an intuitive physical understanding of the significance of a high value of pair correlation between one orientation and another, each orientations being defined by three Euler's angles.

This paper is part of a larger research program aimed at measuring the dimensions of texture heterogeneities nondestructively using ultrasound and to estimate their effect on mechanical properties [10]. Accordingly, in this paper, we propose another method to quantify texture heterogeneities using ultrasound and EBSD. The method provides a description that is less general than the pair correlation function of the orientations, but well-adapted to comparing EBSD and ultrasonic measurements. As we shall see, the method relies on calculating the autocorrelation function of a scalar quantity derived from texture. The characteristic decay length of the autocorrelation function will be associated with the characteristic dimensions of the texture heterogeneities, or macrozones. Built into the method, there will be an implicit, measurement-based definition of macrozones: the volume of material in which the direction of the c axes of the grains remains correlated. Other quantities could be used to estimate macrozone dimensions. Our choice is guided by our desire to compare ultrasonic and EBSD data.

1.2 Ultrasonics

To better study the effect of texture heterogeneities, or macrozones, on mechanical properties, it would be very useful to characterize them non-destructively prior to mechanical testing or service applications. A non-destructive technique would make it easier to correlate macrozones characteristics and mechanical

properties. Ultrasonics is a preferred non-destructive method for bulk microstructural characterization because it is relatively inexpensive and because it allows probing the interior of objects, including metals.

Some researchers have studied the effect of texture heterogeneities on ultrasound propagation, usually with the goal to obtain accurate measurement of ultrasonic attenuation, or to understand the mechanism causing the backscattered ultrasound amplitude in order to minimize it [13-16]. This, in turn, was usually done to improve the capability and the reliability of defect detection. For example, Margetan and al. [13,14] present a C-scan image of the measured back-surface echo amplitude of a titanium plate, 6.35 mm thick, containing enlarged grains. The image shows unexpected amplitude fluctuations. The authors observed some resemblance with the macrozones but they did not assess the macrozone dimensions. Instead, they concluded that the measured ultrasound attenuation (or amplitude fluctuations) arises from beam distortion caused by the microstructure. Similar work was done by Blodgett and Eylon [15] except that they detected the ultrasound with a laser interferometer instead of a piezoelectric transducer. Again, beam distortions were used to explain the larger-than-expected ultrasonic attenuation measured with larger piezoelectric detector. The authors also noted that these distortions were related to the presence of elongated macroscopic inhomogeneities, or elongated grain colonies, aligned in the same directions. The EBSD work described previously tells us that these macroscopic inhomogeneities are likely caused by macro-regions of preferential texture. The sound velocity in hexagonal materials depends on the orientation of the c-axis. In adjacent macrozones the c axes are likely oriented in different macroscopic directions and the propagation velocities of elastic waves should differ from one macrozone to the next. This causes the observed beam distortions.

Acoustic microscopy has also been used to image grains at the surface materials by using, as a contrast mechanism, the surface acoustic wave velocity dependence on the propagation direction with respect to the crystallographic axes [17]. More recently, laser-ultrasonics was used to replace an acoustic microscope. The authors obtained separate EBSD orientation images and ultrasonic images in titanium alloys that showed very similar features [18]. However, they did not identify the regions of uniform velocity with macrozones nor estimate their dimensions. Our group needed a bulk ultrasonic measurement, as

opposed to a surface measurement technique, because we needed to probe the interior of parts nondestructively.

Our work was motivated by a different goal: the need to obtain a non-destructive technique capable of measuring the dimensions of macrozones in the bulk. On the other hand, our work was impaired by the difficulty to measure these dimensions with some reliable reference method. In a previous paper, we showed how difficult it can be to measure these dimensions by optical, metallographic techniques [19]. A solution was found by calculating the 2-dimensional autocorrelation function of the texture-sensitive optical image obtained after macro etching.

In this paper, we briefly disclose a novel, non-destructive, objective, and quantitative ultrasonic technique based on measuring velocity fluctuations as a function of position [20] and we argue that the spatial autocorrelation function of the velocity fluctuations is related to some spatial autocorrelation function of texture heterogeneities. However, the full details of the ultrasonic technique will be submitted for publication later.

The experimental results clearly show that the autocorrelations obtained from the ultrasonic and the EBSD data decay exponentially. The decay length leads to a natural, quantitative, and objective definition of the dimensional characteristics of macrozones. The decay lengths of the spatial autocorrelation function of the EBSD and ultrasonic images are then compared and found consistent with each other for two samples of near-alpha titanium alloy IMI834. The paper includes a discussion on the generality of the results and a discussion on whether these measurements correspond to the "true" macrozone dimensions.

2. Experimental procedure

2.1 Material

Two parallelepipeds referred to as sample S1 and S2 were cut from a forged disk of near-alpha titanium alloy IMI 834. The x, y, and z dimensions (width x height x thickness) of the parallelepipeds were equal to $34 \times 27 \times 9$ mm^3 and $25 \times 17 \times 7$ mm^3. S1 was cut close to the contact surface between the billet and the

die (region often called 'dead zone' as it receives very little deformation from the forging process). S2 was cut just below, in a region that had undergone deformation.

The samples' microstructure consisted of approximately 30% equiaxed α_p grains surrounded by α_s laths with thin β layers between them. The equiaxed α_p grain size was about 25 µm, whereas the width of the α_s laths was around 1-2 µm. More information about the microstructures can be found elsewhere [4].

Ultrasonic and EBSD measurements were made on the largest (XY) surface. In addition, a (YZ) section was cut in the middle of each parallelepiped for additional EBSD measurements in a plane perpendicular to XY plane.

2.2 EBSD measurements

EBSD analyses were performed either using the JEOL JSM-6500F microscope equipped with the Standard Channel 5 EBSD System (HKL technology) or using the JEOL JSM-6490 microscope equipped with the Fast Acquisition EBSD System (HKL technology). The EBSD samples were polished down to a 4000 grit silicon carbide paper followed by a final polishing with a mixture of colloidal silica and hydrogen peroxide [8]. Very large XY and YZ surfaces of the two samples were measured by stitching adjacent orientation maps obtained in beam controlled mode. From these EBSD data, which describe the orientation at each pixel location, different crystallographic characteristics can be calculated. The colors in Fig. 1, according to the code displayed in Fig 1e, show the sample's thickness direction, Z, in relation to the crystal directions. The surface areas are of order 1 cm^2 and the pixel dimensions are between 10 and 15 µm. The rapid color variations are due to rapid variations in crystallographic orientation (texture) from grain to grain. The large scale variations in shades produced by the dithering effect of the rapidly changing colors are caused by local textures, i.e. by the macrozones.

The only universally agreed feature of macrozones is that they are some kind of texture heterogeneities. However, from EBSD images such as those shown in Fig. 1, it is difficult to draw clear boundaries between dithered regions and therefore evaluate macrozone dimensions. Furthermore, the color scale shown in Fig. 1e is highly nonlinear in the sense that in some regions of the color scale, a small change in

orientation produces a large visual contrast, and in other regions of the color scale, a similarly small change in orientation produces a small visual contrast. Therefore, it is likely that the apparent boundaries between regions of different colors are as much an artifact of the color scale as a representation of the true boundaries of regions of different local texture (unless it is known *a priori* that there are only 3 possible orientations corresponding roughly to the 3 apex of the color triangle, with little scatter around them, and that the color scheme was designed for that purpose). This does not mean, however, that the different regions are a visual artifact. They do represent real changes in local texture. But it means that some boundaries may not be where they seem to be, and other boundaries may be missing or artificially introduced by the color scale. This discussion should not be interpreted as a limitation of EBSD. EBSD is probably the best technique for microtexture analysis. However, the representation of the data of Fig. 1 is common, and inferences about macrozone dimensions are made from such representations.

For example, it seems qualitatively obvious that the mean macrozone orientation and sizes of the two samples are different (Figs. 1a vs. 1c). In the YZ plane, the macrozones are aligned approximately 8° and 22° away from the Y axis for samples S1 and S2, respectively. Also, in the X direction, the macrozones are wider for sample S2 than for sample S1. However, as discussed above, it would be difficult to estimate macrozone size quantitatively. Later in this paper, we will attempt to quantify these same macrozone characteristics using a different representation of the EBSD data.

2.3 Ultrasonic measurements

In this section, we disclose a novel ultrasonic method capable of estimating the dimensions of macrozones [20]. In a single crystal, the sound velocity (or elastic constant) depends on the propagation direction. In a polycrystalline aggregate, the sound velocity (or effective elastic constants) is some mean of the sound velocity (or elastic constants) averaged over all possible orientations of the crystallites [21,22]. However, when the crystallites (i.e. the grains) are few in the volume probed by the ultrasound, one expects that the measured velocity will be close to the mean value, but fluctuating around it for different probing locations. The fluctuation is caused by size and orientation variations of the finite number of grains. The larger and fewer are the grains, the larger are the fluctuations. Exploiting this idea, the

measurement consists in probing as small a volume as possible and imaging velocity fluctuations as a function of probing position.

Figure 2 is a schematic diagram of the measurement setup. A water immersion tank is employed. A 10 MHz transducer of 12.7 mm (0.5 inch) diameter, 32 mm (1.25 inch) focal length is positioned such that its axis is normal to the surface and its focal point is located at the sample surface. In water, the acoustic wavelength at 10 MHz is approximately 0.15 mm and the calculated beam diameter at the focal point (diameter at half maximum amplitude) is 0.19 mm. The transducer is used both as a source and a detector of ultrasound. Only longitudinal waves are used (no transverse, or shear, waves). Because of the geometrical configuration, the transducer is highly sensitive to ultrasound propagating along a path perpendicular to the surface. Other ultrasonic paths lead to strong destructive interference and negligibly small signal amplitude compared to the main path. Therefore, the probed volume is equal to the focal point area times the sample thickness. In our case, this is $0.028 \times 7\ mm^3$ for sample S1. If the macrozones have dimensions of the order of 1-2 mm then, for a plate of less than 10 mm thickness, the ultrasound beam may encounter only five to ten macrozones. As a consequence of this small number of regions, the average sound velocity will be close to, but probably not equal to, the mean velocity averaged over an infinite number of macrozones. Therefore, this small volume should show measurable velocity fluctuations with a lateral resolution equal to 0.19 mm.

The measurement principle is illustrated schematically in Fig. 2b for a plate of material containing macrozones of arbitrary shapes. As the transducer is scanned along path 1, then 2, 3, and 4, one can see that initially, the sound wave will traverse similar regions of the material (paths 1 and 2). The regions traversed will differ somewhat more along path 3. They will be completely different along path 4. Clearly, the length scale over which the sound velocity becomes uncorrelated with the velocity measured along path 1 is an estimate of macrozone dimensions. This argument is independent of sample thickness. Sample thickness will influence the magnitude of the velocity fluctuations, but not the distance over which velocity correlates with itself. Later in this paper, we will discuss how this idea can be used to quantify macrozone dimensions using ultrasonic data.

3. Analysis and Results

3.1 EBSD

The orientation information obtained from EBSD together with the single crystal elastic stiffness constants and density of titanium (c_{11} = 162.4, c_{33} = 180.7, c_{12} = 92.0, c_{13} = 69.0, c_{44} = 46.7 GPa, and density = 4506 kg/m^3)[23] were used to calculate the sound velocity in the Z direction, which is also the propagation direction of the ultrasound in the setup of Fig. 2. The resulting maps are shown in Fig. 3. The gray scale is adjusted so that black and white correspond approximately to the minimum and maximum theoretical value (6003 m/s in the basal plane and 6332 m/s in the direction of the c axis), respectively.

Fig. 3 shows that the sound velocity calculated from the EBSD data varies greatly within the sample, from the minimum to the maximum possible theoretical values. The average grey level of all four figures is about the same. Indeed, the calculated mean velocities for Figs. 3a through 3d are 6096, 6080, 6072, and 6085 m/s, respectively. As expected, the mean velocities calculated from each of the two planes of a single sample (Sample S1 in Figs. 3a and 3b and sample S2 in Figs. 3c and 3d) are close to each other.

The grey scale patterns of Fig. 3 present great similarities with the color patterns of Fig. 1. Qualitatively, one can still recognize the macrozone patterns of Fig. 1 (elongated in the Y direction in both samples). It should be noted here that the sound velocity of hexagonal materials depends only on the angle between the propagation direction and the c axis of the material according to well-known equations [24]. Therefore, if in Fig. 3 one had represented this angle by the gray scale, this other version of Fig. 3 would not be very different. Therefore, it is precisely because the ultrasonic velocity is so closely linked to orientation information that Fig. 1 and Fig. 3 are so similar. Nevertheless, the images are not equivalent because pixels of different colors in Fig. 1 (such as the [-12-10] and [01-10] directions that are represented by green and blue pixels, respectively) can correspond to the same ultrasonic velocity (6003 m/s) in Fig. 3.

In Fig. 3, the three-dimensional orientation information has been reduced to a scalar, the sound velocity. It is now easy to calculate the two-dimensional autocorrelations of these figures using commercial software. Because we are interested in velocity fluctuations, as opposed to absolute velocity, the mean velocity is subtracted from the images prior to calculating the autocorrelation. And because the

autocorrelation varies by orders of magnitude, its value was plotted on a log scale in units of dB, where the 0 dB value is defined as the maximum of the autocorrelation.

The results are shown in Fig. 4 where the 2-dimensional color-coded graphs represent the amplitude of the autocorrelation as a function of the two spatial dimensions. Superimposed and centered on the graph are two perpendicular white lines, one nearly vertical and the other nearly horizontal. They are rotated until one of them is aligned with the direction of highest correlation amplitude. The lines define two perpendicular 1-dimensional sections that are illustrated to the right of the 2D color graphs.

All sections show the same basic features but these features are most striking in the sections along the high correlation (vertical) direction. All sections consist in a narrow center peak followed by a linear decrease as a function of distance. The half-width at half-maximum of the narrow central peak is approximately 20 μm, i.e. barely more than one pixel (15 μm). This sharp center peak reflects that the orientation changes rapidly on that scale because the α_p grain size is about 25 μm and because the α_s laths are organized into colonies of comparable dimensions.

Near -20 dB, the sections change to a highly linear dependence (on the semi-log plot) until the signal reaches the noise level. The linearity remains for 20 to 40 dB on the vertical axis, i.e. over up to two orders magnitude in amplitude. Therefore, the autocorrelation decreases exponentially over distances measured in mm. Table 1 shows the fitted decay length, x_0, defined as

$$A = A_0 \exp -(x/x_0)$$

where A is the autocorrelation amplitude and A_0 is fitted and approximately equal to 0.1 (-20 dB). It should be noted that the measured decay lengths of the two samples are not very different in the long direction, but they differ by a factor of 2 to almost 4 in the short directions, and the orientation of the macrozones are quite different.

An additional feature can be noted on some of the sections along the low correlation directions. The feature is most obvious in Fig. 4b where sharp peaks are observed at ± 2 mm in the section close to the Z direction. These peaks indicate some level of spatial periodicity in the sound velocity and texture.

Similarly, there appears to be some periodicity close to the X direction with a period of 2.8 mm in Fig. 4a and a periodicity close to the Z direction with a period of 1.1 mm in Fig. 4d. The periodicity can be made more obvious by doing an autocorrelation on a narrow strip as opposed to the entire images of Fig. 3, and it is possible to obtain harmonics of that period.

3.2 Ultrasound

Figure 5 maps the fluctuations of the ultrasonic propagation delay (in μs) in the Z direction as a function of position (in mm) in the XY plane. The measured area is larger than that measured by EBSD and includes the area measured by EBSD. The images of the fluctuations resemble those calculated by EBSD (Figs. 3a and 3c) but the images clearly do not have the same spatial resolution. Both images show elongated structures aligned close to the vertical axis and the structures are coarser for sample S2. To estimate the spatial dimensions of the fluctuations, the two-dimensional autocorrelation of the delay fluctuations were calculated (Fig. 6).

The EBSD and ultrasonic results obtained in the XY planes for the same samples can be compared using Figs. 4a and 6a for sample S1, and Fig. 4c and 6b for sample S2. In contrast with Fig. 4, Fig. 6 shows no sharp central peak corresponding to the step size. This is because the ultrasonic measurement resolution is coarser and because the measurement averages the sound velocity over a cylindrical volume of approximately 0.19 mm in diameter times the thickness of the sample (7 or 9 mm). In this volume, there are a very large number of grains and their effect is averaged precisely. Moreover, the step size is 0.125 mm and the delay measurement was very precise (not noisy). So there was essentially no pixel-to pixel variation caused by the microstructure or by measurement errors. However, there was a small number of macrozones probed along each path. This created the velocity fluctuations shown in Fig. 5 and the decays of the autocorrelations shown in Fig. 6.

The sections made along the direction of high correlation, close to the vertical axis in Fig. 6, show an exponential decay similar to that observed with EBSD. However, the decay lengths are different: 6.22 and 4.31 mm for ultrasound, as opposed to 0.83 and 0.78 mm for EBSD, for samples S1 and S2, respectively (Tables 1 and 2). The horizontal sections are in the directions of short correlation distance and it is

difficult to estimate the decay lengths. Nevertheless, they are indicated in Table 1. Figs. 6a and 6b show nearly the same values of x_0, which is counter intuitive when looking at Fig. 5. The values of x_0 measured with both techniques differ by a factor of 2 for sample S2, and even more for sample S1. However, the resolution of the ultrasonic measurement (estimated at 0.19 mm) is too coarse to allow a measurement as small as that found with EBSD for sample S1. Also, like Fig. 4a, Fig. 6a shows a quasi periodicity in the horizontal direction with a period of approximately 3 mm. Unlike Fig. 4c, however, Fig. 6b shows a periodicity in the horizontal direction with a period of 4.6 mm.

Although they show similar overall features, they differ quantitatively. With EBSD, a single pixel represents the calculated velocities in a precise location on the measurement plane. In contrast, with the ultrasonic data, a single pixel represents the delay (inverse velocity) averaged in the entire thickness of the sample. Because the delay fluctuations are so small, they are linearly related to velocity through the Taylor approximation, $\Delta v = -v\Delta t$, where t is time delay, Δt is delay fluctuation, v is velocity, and Δv is velocity fluctuation. Therefore, it is important to realize that the EBSD and ultrasonic autocorrelations differ in that the EBSD measurements allows to calculate velocity on a plane of zero thickness, whereas the ultrasonic measurements are averaged through the entire sample thickness. This is why the EBSD and ultrasonic autocorrelations resemble each other but yet they are different.

4. Discussion

4.1 Exponential autocorrelation functions arising from EBSD data

The ultrasound velocities calculated from the local texture contains, of course, less information than the texture itself but is illustrative of it. This scalar value is much easier to handle mathematically and we could apply a simple two-dimensional autocorrelation to our data instead of using the more complex procedure of Gao et al. [12].

That the autocorrelation of the sound velocity fluctuations calculated using the EBSD data is so closely exponential over approximately 2 orders of magnitude is rather surprising. Why would such a mathematical construct on complex EBSD data have such a simple property? Moreover, to our knowledge, no exponential decay of the autocorrelation of a texture-related quantity has ever been

reported. It must be noted, however, that EBSD maps are rarely made over large areas such as those reported herein, and this may explain why this striking observation has never been made.

The exponential decay obtained from EBSD data implies other exponential decays. Let v_{ij} be some sound velocity, M_{ij} be some elastic modulus, and ρ be the density, such that

$$v_{ij}^2 = M_{ij} / \rho$$

Here, the indices indicate that the ultrasound is propagating in the direction i and polarized in the direction j. Also, let

$$v_{ij} = v_0 + \Delta v_{ij}$$

$$M_{ij} = M_{0+} \Delta M_{ij}$$

It is easy to prove that the spatial autocorrelation of $\Delta v_{ij} / v_0$ is equal to one half the autocorrelation of $\Delta M_{ij} / M_0$ in the limit $\Delta v_{ij} / v_0 << 1$. This limit is satisfied because the velocity fluctuations, Δv, are approximately ±165 m/s for a mean velocity, v_0, of approximately 6165 m/s, so that $\Delta v / v_0 \approx 3\%$. Therefore, the exponential decay of the autocorrelation of the sound velocities implies that the autocorrelation of M_{ij} is also an exponential decay with the same decay length. This result is worth mentioning because the link between elastic constant fluctuations and texture heterogeneities is somewhat more direct (it does not depend on density). Also, it shows that the exponential decay may be not an accident but a more general feature.

This observation of highly accurate exponential decays begs for an explanation. In [25], we read "The exponential correlation function is a natural correlation in one dimension, since it corresponds to a Markov process. In two dimensions this is no longer so, although the exponential is a common correlation function in geostatistical work." Therefore, if we had observed the exponential function in a one-dimensional correlation, we would have concluded that the texture at some position x depends to some extent on texture in the interval $x \pm \Delta x$, where Δx is some distance beyond which there is no more dependency. Said differently, a Markov process is a process in which there is complete de-correlation of

the information beyond some distance. By definition of a macrozone (macro regions with a strong texture component, see introduction), texture remains correlated with itself within the same macrozone, but may or may not be correlated outside the macrozone. The exponential decay of the autocorrelation function therefore would be explained if beyond some distance texture becomes un-correlated. So we come to an important result: If we assume that the relative orientation of two adjacent macrozone is random, then the decay length of the autocorrelation function is an estimate of macrozone dimension. This estimate is quantitative and unambiguously defined. Moreover, it is an objective estimate in the sense that it follows from a mathematical procedure and does not depend on the judgment of an observer.

Lastly, in the Markovian texture assumption, several quantities derived from texture (such as sound velocity) will be un-correlated beyond some distance. Their autocorrelation functions will be exponential, although the decay length might vary depending on what quantity is calculated from the texture information.

In summary, this discussion demonstrates that under the Markovian texture assumption, the autocorrelation function of quantities derived from texture, such as the sound velocity, is exponential and the decay length is an estimate of the correlation length (or characteristic dimension). Different estimates might be obtained depending on which quantity is utilized in the autocorrelation (we did not investigate this aspect further), but autocorrelations of sound velocities and of the corresponding combination of elastic constants will give identical estimates.

Therefore, a natural definition of macrozone dimension arising from EBSD measurements is the correlation length of a scalar quantity calculated from the measured texture. Here, this scalar quantity is the calculated sound velocity in the Z direction.

4.2 Exponential autocorrelation functions arising from ultrasonic data

The exponential decay of the sound velocity autocorrelation was observed over only one order of magnitude. However, Fig. 6 shows that if the dimensions of the scan had been larger, the decay would have continued probably further. While describing Fig. 2b, it was argued that the average sound velocity on a straight path though the sample thickness should be correlated with itself for two path sufficiently

near each other. Conversely, the average sound velocities on two paths separated by a distance larger than macrozones dimensions should be uncorrelated. We can formalize this argument somewhat better now. Assuming that the directions of the c-axes in the macrozones are uncorrelated beyond some distance, then the velocity fluctuations must be uncorrelated beyond that same distance and the autocorrelation function of the velocity fluctuations must be an exponential function. In fact, because the sound velocity only depends on the orientation of the c axes of the crystallites with respect to the Z direction of the sample, only the orientation of this axis (as opposed to rotations around the axis) needs to be uncorrelated beyond some distance to render exponential the spatial autocorrelation of the velocity fluctuations.

The decay length of the ultrasonic correlation function may or may not be identical to that obtained from the EBSD measurements because the ultrasonic and EBSD measurements are different. The EBSD data (converted to velocities or not) considers only points on a 2D plane within the sample, while the ultrasound is an average velocity along a path. However, both are based on the same underlying governing feature, i.e. the correlation length of texture heterogeneities. Therefore, the decay length of the autocorrelation of the ultrasonic data should be proportional to that found from EBSD data, with a proportionality constant of order 1. The ultrasonic data does indeed show an exponential decay of the autocorrelation function in one of the two spatial dimensions. In the other dimension, the estimate spatial resolution of the measurement (0.19 mm) is more than one fifth of the decay length (0.89 mm or less) and the decay length is difficult to measure precisely.

4.3 Self-consistency of the dimensions deduced from EBSD measurements

Clearly, the qualitative and quantitative information obtained from EBSD regarding the dimensions of the macrozones show that they are elongated in the Y direction and narrow in the other two directions. In addition, the long dimension is inclined with respect to the XY plane, as is readily apparent from the YZ plane measurement. To obtain the true dimensions of the macrozones, it would have been necessary to cut the sample surfaces along planes in which the principal dimensions lie. The argument is the same as for standard metallography measurements of grain size when the grains are elongated. To observe the true dimensions of grains, the metallographic planes must be aligned with the principal dimensions of the

grains. Therefore, the velocities calculated from EBSD measurements underestimate the decay length y_0 in the long dimension (Y direction).

Two measurements of y_0 were obtained by EBSD for each sample, as shown in Table 1. The redundancy can be used to check the self-consistency of the measured data. Let's assume that the macrozones have the shape of a rod-like parallelepiped. We would expect this for the un-deformed billet and for the lightly deformed sample S1. Then, the value of y_0 measured in the XY plane, $(y_0)_{XY}$, is related to z_0 as measured in the YZ plane provided that the YZ plane provides a true estimate of z_0 (Fig. 7). Because z_0 is short and because the macrozones form a small angle of $\theta_{XY} = 5^\circ$ with respect to the YZ plane, then the measured value of z_0 is probably accurate. Fig. 7. shows that in the limit of large y_0,

$$(y_0)_{XY} = (z_0)_{YZ} / \sin(\theta_{YZ}).$$

Substituting for $(z_0)_{YZ} = 0.12$ mm and $\theta_{YZ} = 7^\circ$, we obtain $(y_0)_{XY} = 1.0$ mm for sample S1. This is close to the value of 0.83 mm obtained in the XY plane. Similarly, the value of y_0 measured in the YZ plane, $(y_0)_{YZ}$ is related to x_0 measured in the XY plane by

$$(y_0)_{YZ} = (x_0)_{XY} / \sin(\theta_{XY}).$$

Substituting for $(x_0)_{XY} = 0.10$ mm and $\theta_{XY} = 5^\circ$, we obtain $(y_0)_{YZ} = 1.15$ mm, which can be compared to the value measured in the YZ plane, 1.44 mm. The two values are relatively close, considering that a 1° error in θ_{YZ} would raise $(y_0)_{XY}$ to 1.43 mm, considering that a small amount of curvature can be observed in Figs. 3a and 3b, and considering that the two samples were not taken at the exact same location. For sample S2, these two self-consistency arguments cannot bet made because the estimated dimensions in Table 1 show that the macrozones may no longer be rod-like and because they are elongated in a direction relatively far from the axes.

This self-consistency argument for Sample S1 reinforces the validity of the characteristic dimensions estimated by EBSD. In conclusion, the decay lengths of the autocorrelation function would have given the dimensions of the macrozones if the inspection planes had been aligned with the principal dimensions of

the macrozones, just as metallographic images reveal the true dimensions of elongated grains only when the image planes are aligned with the principal dimensions of the grains.

4.4 Comparison of macrozone dimensions obtained from EBSD and ultrasonic measurements

There remains to discuss the original goal of the paper: Does the ultrasonic measurement really measure the dimensions of the macrozones? As demonstrated in section 4.4, the characteristic dimensions measured by EBSD were not the true macrozone dimensions because the measurement planes were not aligned with the macrozones. Fig. 7 shows that the EBSD measurements produce only a lower bound estimate of the macrozone dimensions because there is no guarantee that the EBSD image plane is aligned with the principal axes of the macrozones. Accordingly, the EBSD estimates are indeed lower than the values measured by ultrasonics. In contrast, the ultrasonic measurements are averaged through the entire thickness. To a first approximation, they are insensitive to a small angle of the macrozones with respect to the measurement plane because the measurement is sensitive to the projection of the dimensions onto the measurement plane. For small angles, the projection has essentially the same length as the true length. So it is expected that the characteristic dimensions obtained by ultrasonics are close to the macrozone dimensions. In addition, both techniques gave the same estimate of macrozone angles to within 2 degrees (probably due to sample positioning accuracy) for sample S1. For sample S2, Fig. 3c qualitatively shows that different regions may have somewhat different orientations, and this may explain the why there is a difference of 12 degrees between EBSD and ultrasonic measurements of orientation.

4.5 Limitations and usefulness

One limitation of the ultrasonic measurement as compared to EBSD measurements is that its resolution is limited to decay length larger than approximately 1 mm (a few times the spatial resolution of 0.19 mm). On the other hand, EBSD measurements over large dimensions such as those shown in this paper are extremely time consuming and EBSD is therefore better suited for smaller decay lengths. So EBSD and ultrasonics complete each other in this point of view.

As discussed in section 4.1, we expect that the autocorrelation of various parameters derived from texture heterogeneities will decay exponentially as long as texture is uncorrelated beyond some distance.

However, the decay length may vary somewhat depending on which quantity is derived from the texture information. Also, it is theoretically possible that some component of texture be randomized on a length scale that is different from that of some other texture component. In such cases, the reduction of the complete texture information to two different scalar parameters might yield two different estimates of macrozone dimensions.

From an ultrasonic point of view, it is usually easiest to measure the longitudinal velocity in the thickness direction and this automatically determines which texture-related scalar quantity is measured. However, using combinations of longitudinal and transverse waves would allow some freedom of choice. For example, for cubic materials, it is possible to measure independently two, fourth order texture coefficients by using three such waves propagating in the thickness direction [26]. These two texture coefficients might be representative of texture components with different correlation lengths. Therefore, whether the data is obtained by ultrasound or EBSD, it is imperative that the scalar quantity used to create the 2D map and the corresponding autocorrelation graphs be unambiguously defined.

Finally, it is important to keep in mind that defining the macrozone dimensions as the characteristic dimensions of the decay length of scalar quantities derived from texture is a pragmatic definition. This choice may not correspond to the "true" dimensions, but it enables objective and quantitative estimates using available measurement tools.

On the other hand, the representation of a dimension by the characteristic decay length of an autocorrelation function is not new. A well-established theory relating grain size to ultrasonic properties [22] assumes that grain size can be represented by a geometrical autocorrelation function. When solving the inverse problem of measuring grain size using appropriate ultrasonic methods, the fitted characteristic length is a good estimator of grain size [27]. For those familiar with this theory, estimating macrozone dimensions from an autocorrelation function based on texture should not be a strange concept.

The measurement of macrozone dimensions proposed herein can and should be used to attempt to build new structure-property relationships for titanium alloys. In a previous paper [10], some the present authors showed how the mean ultrasound velocity, which depends on texture, correlated with dwell-

fatigue life for six near-alpha titanium samples. However, a sixth one did not. The sixth one happened to be the one with a substantially coarser "local texture variations" as imaged with the present ultrasonic technique. But, at the time, the authors felt it was premature to extract macrozone dimensions with confidence from the data. It was felt that the work contained herein was required before going further ahead.

4.6 Quasi-periodic microtexture fluctuations

In addition to the exponential decay of the autocorrelation which has led us to a definition and a measurement method of the macrozone dimensions, we have also noted that some sections in Fig. 4 display lateral peaks that were interpreted as a quasi-periodicity in the texture information. Therefore, the process by which the sample was made produced a texture more complex than a Markovian texture. The texture heterogeneities are not completely uncorrelated beyond some characteristic distance and do not satisfy our Markovian assumption for estimating macrozone size. Instead, the macrozones appear to become uncorrelated after a short distance and to become correlated again some distance away. How can this be?

Presently, we do not know how this quasi-periodicity was created. There exist metallurgical processes that can create large scale microtexture fluctuations. For example, these long distance fluctuations of local texture might be related to the hot deformation of the beta phase during the early stage of the forging process (BCC materials are known to generate alternating bands of two texture fibers) [28]. Or they could be related to some variant selection effect and subsequent coupling of the two phase microstructure during cooling below the beta transus. In any case, these alternating structures would not have disappeared completely by randomization in the subsequent processing steps. Therefore, the observation of a quasi-periodicity is believable.

4.7 Comment on ultrasound scattering and the validity of the ray tracing approximation

The color contrast observed in Figure 5 was explained in Section 2.3 as caused by variations in the mean ultrasound velocity along a linear ultrasonic path, i.e. in the ray tracing approximation. Is this assumption

valid or is the ultrasound scattered so that the ultrasound does not necessarily propagate along a straight path?

The acoustic wavelength at 10 MHz is approximately 0.6 mm. Therefore, the acoustic wave is scattered negligibly by the rapid grain-to-grain variations occurring on the scale of 1-25 μm, and it travels at a speed that is some average of the local velocity. However, the acoustic wave should be scattered by the large scale variations identified with the macrozones because these variations occur over dimensions comparable to the acoustic wavelength. In fact, it is well documented that such large scale variations in local texture do affect ultrasound propagation. For example, in a past paper, we showed that large scale texture variations explain why sample S1 has larger backscattered ultrasound amplitude than sample S2 for ultrasound propagating in the X direction [16]. These large scale variations of texture and velocity are also the source of signal amplitude fluctuations observed by other authors [13-15].

The amplitude of the randomly scattered ultrasound that reaches the detector is small and does not interfere with the measurement of the propagation delay. However, the amplitude of the forward scattered (i.e. scattered without changing propagation direction significantly but by acquiring a phase shift) ultrasound could be significant and could contribute to the measured signal propagation delay when the unscattered and scattered waves are summed up. This would cause a phase shift and affect the time delay measurement. However, the two model descriptions (ray tracing vs. forward scattering) are not incompatible. Although the link between the two descriptions is not obvious, the phase shift caused by the forward scattered ultrasound can be viewed as a change in velocity. So although the ray tracing model may be considered too simple, it provides an adequate explanation for the purpose of this paper.

Conclusion

EBSD and ultrasonic measurements of macrozone dimensions were made on two samples of near-alpha IMI834 titanium alloy. The EBSD measurements were made on two perpendicular planes over areas much larger than what is usually done. The measured orientations were used to calculate the sound velocity at each point of the maps. In reducing the information to such a scalar value, which closely depends on the angle that the single crystal c axes make with the Z direction, it was easy to perform a 2-

dimensional autocorrelation. The autocorrelation had an exponential decay characteristic of Markovian structures, i.e. of structures that loose memory of themselves beyond a certain distance. Markovian behavior is commonly encountered in nature so this led us to define, in a fairly general manner, the characteristic dimensions of the texture heterogeneities, or macrozones, as the characteristic decay length. Implicit in this definition of macrozone dimension is the assumption that macrozones are Markovian texture heterogeneities. To our knowledge, this is the first time that macrozone dimensions can be measured objectively and quantitatively. However, it was shown that the characteristic lengths deduced from the velocity variations calculated from EBSD data were lower than the true dimensions because the macrozones were inclined with respect to the EBSD measurement planes. The true characteristics lengths would be obtained if the measurement planes were cut along the principal dimensions of the macrozones.

A novel, nondestructive, ultrasonic measurement technique to measure macrozone dimensions was disclosed. The technique is based on the measurement of the fluctuations of ultrasonic propagation delay of bulk waves. The autocorrelation of these fluctuations also showed an exponential decay from which characteristic dimensions of macrozones were obtained. In contrast with EBSD or acoustic microscopy measurements, the ultrasonic measurement projects the texture information averaged over the entire thickness of the sample onto the measurement plane. Because of this, the ultrasonic characteristic dimensions are expected to better reflect the true dimensions of the macrozones when these are inclined.

The measured spatial orientation of the macrozones with respect to the principal directions were roughly the same using both Ultrasonic and EBSD measurements. In addition, both techniques showed that the macrostructures are sometimes semi-periodic in the directions of the short dimensions, and both techniques indicated that the period was about 2.9 mm for sample S1 in the X direction. To our knowledge, it is the first time that such quasi-periodic structures in texture are objectively reported by EBSD or ultrasonics.

Acknowledgements

The first two authors thank Daniel Lévesque and Harold Hébert for their help. Funding of the ultrasonic work was provided in part by the Natural Science and Engineering Research Council of Canada.

Tables and Table captions

Table 1. Autocorrelation decay length, x_0, y_0, and z_0 in the direction close to the X, Y, and Z directions, angle from that direction, and periodicity, as obtained by EBSD and Fig. 4.

Sample	Plane	x_0 (mm)	y_0 (mm)	z_0 (mm)	Angle (Degrees)	Periodicity (mm)
S1	XY	0.10	0.83	---	5	2.8
S1	YZ	---	1.45	0.12	7	2.0
S2	XY	0.37	0.80	---	18	---
S2	YZ	---	1.36	0.20	23	1.1

Table 2. Autocorrelation decay length, x_0 and y_0 in the direction close to the X and Y directions, angle from that direction, and periodicity, as obtained by ultrasonics and Fig. 6.

Sample	Plane	x_0 (mm)	y_0 (mm)	Angle (degrees)	Periodicity (mm)
S1	XY	0.89	6.1	3	3.0
S2	XY	0.86	4.3	11	4.6

References

[1] Woodfield AP, Gorman MD, Sutliff JA, Corderman RR. Effect of microstructure on dwell fatigue behaviour of Ti-6242, Proc of the 8th World Conf on Titanium. Birmingham, UK, October 22–26 (1995), 1116–1123.

[2] Le Biavant K, Pommier S, Prioul C. Local texture and fatigue crack initiation in a Ti-6Al-4V titanium alloy. Fatigue and Fracture of Eng. Mater. & Structures 2002;25:527-47.

[3] Panetta PD, Thompson RB, Margetan FJ. Use of electron back scatter diffraction in understanding texture and the mechanism of back scattered noise generation in titanium alloys. Rev of Prog in Quant Non Destruct Eval 1998;17A:89-96.

[4] Germain L, Gey N, Humbert M, Bocher P, Jahazi M. Analysis of sharp microtexture heterogeneities in a bimodal IMI 834 billet. Acta Mater 2005;53:3535-3543.

[5] Humbert M, Germain L, Gey N, Bocher P, Jahazi M. Study of the variant selection in sharp texture regions of bimodal IMI 834 billet. Mat Sci & Eng A 2006;430:157-64.

[6] Germain L, Gey N, Humbert M, Vo P, Jahazi M, Bocher P. Texture heterogeneities induced by subtransus processing of near α titanium alloys. Acta Materialia 2008;56:4298-4308.

[7] Bache MR. A review of dwell sensitive fatigue in titanium alloys: the role of microstructure, texture and operating conditions. Int J Fatigue 2003;25:1079-1087.

[8] Uta E, Gey N, Bocher P, Humbert M, Gilbert J. Texture heterogeneities in titanium forging analyzed by EBSD - Relation to Fatigue Crack Propagation. J Microscopy 2009;233(3):451-459.

[9] Bridier F, Villechaise P, Mendez J. Analysis of the different slip systems activated by tension in a α/β titanium alloy in relation with local crystallographic orientation. Acta Mater 2005;53:555-567.

[10] Toubal L, Bocher P, Moreau A. Dwell-fatigue life of a near-alpha titanium alloy and ultrasonic measurement correlation. 12th International Conference on Fracture, Ottawa (2008).

[11] Wright SI, Field DP, Witt R, Michaluk CA. On the development of new scalar measures of heterogeneity. Mater Sci Forum 2002;408-412:107-112.

[12] Gao X, Przybyla CP, Adams BL. Methodology for recovering and analyzing two-point par correlation functions in polycrystalline materials. Metallurgical & Mater Trans A 2006;37A:2379-2387.

[13] Margetan FJ, Gigliotti M, Brashe L, Leach W. Fundamental studies: Inspection properties for engine titanium alloys. U.S. Department of Transportation & Federal Aviation Administration Report DOT/FAA/AR-02/114, December 2002.

[14] Yu L, Margetan FJ, Thompson RB, Degtyar A. Survey of ultrasonic properties of aircraft engine titanium forging. Rev of Prog in Quant Non Destr Eval 2002, 21:1510-1517.

[15] Blodgett MP, Eylon D. The influence of texture and phase distortion on ultrasonic attenuation in Ti-6Al-4V. J Nondestr Eval 2001;20(1):1-16.

[16] Humbert M, Moreau A, Uta E, Gey N, Bocher P, Bescond C. Analysis of the microstructure and local texture of IMI 834 samples in relation to ultrasonic backscattered noise. Acta Mater 2008; 57(3):708-714.

[17] Lemons RA, Quate CF. Acoustic Microscopy. In Physical Acoustics XIV, edited by Mason WP and Thurston RN (Academic, New York, 1979) p. 1.

[18] Sharples SD, Clark M, Li W, Somekh MG. Rapid imaging of microstructure using spatially resolved acoustic spectroscopy. Proc. Of the 1st Internat. Symp. on Laser-Ultrasonics: Science, Technology and Applications. Montreal Canada, July 16-18 (2008).

[19] L. Toubal, P. Bocher, A. Moreau, and D. Lévesque. Macro-regions size measurements in bimodal titanium forgings using 2D autocorrelation method. Metallurgical & Mater Trans A 2010;41(3):744-750.

[20] Moreau A, Toubal L. Method and apparatus for ultrasonic characterization of scale dependent bulk material heterogeneities. Patent applications filed in U.S.A. Canada and Europe.

[21] Bunge HJ. Texture analysis in materials science. Butterworths and Co., London, 1982.

[22] Stanke FE, Kino GS. A unified theory for elastic wave propagation in polycrystalline materials. J Acoust Soc Am 1984;75:665-681.

[23] Fisher ES, Renken CJ. Single-crystal elastic moduli and the hcp - bcc transformation in Ti, Zr, and Hf. Phys Rev 1964;135 (2A):A482-A494.

[24] An excellent textbook on crystal acoustics is: Auld BA. Acoustic fields and waves in solids, Second edition. Malabar, Krieger, 1990. The equations are found on p. 396-398.

[25] Guttorp P, Gneiting T. Studies in the history of probability and statistics XLIX On the Matérn correlation family. Biometrika 2006;93(4):989-995.

[26] Moreau A, Lévesque D, Lord M, Dubois M, Monchalin JP, Padioleau C, Bussière JP. On-line measurement of texture, thickness, and plastic strain ratio using laser-ultrasound resonance spectroscopy. Ultrasonics 2002;40:1047-1056.

[27] Moreau A, Lord M, Lévesque D, Dubois M, Bussière J, Monchalin JP, Padioleau C, Lamouche G, Veres T, Viens M, Hébert H, Basséras P, Jen CK. AISI/DOE Advanced Process Control Program. Vol. 4 of 6: On-line, Non-destructive Mechanical Property Measurement Using Laser-Ultrasound. American Iron and Steel Institute, 2001. http://www.osti.gov/energycitations/product.biblio.jsp?osti_id=794988.

[28] Song R, Ponge D, Raabe D, Kaspar R. Microstructure and crystallographic texture of an ultrafine grained C–Mn steel and their evolution during warm deformation and annealing. Acta Mater 2005;53(3):845-858.

Figure Captions

Figure 1. Inverse pole figure maps obtained from EBSD data in a) Sample S1, XY plane, b) Sample S1, ZY plane, c) Sample S2, XY plane, d) Sample S2, ZY plane, e) color code. The reference direction is that of the sample's thickness, or Z direction for all figures. All maps are drawn using the same dimensional scale.

Figure 2. Schematic representation of the ultrasonic measurement configuration: a) Ultrasound tank, b) four typical paths across the thickness of a sample.

Figure 3. Calculated sound velocity in the Z direction from EBSD data for a) Sample S1, XY plane, b) Sample S1, ZY plane, c) Sample S2, XY plane, and d) Sample S2, ZY plane. The gray scale (e) represents the ultrasound velocity in units of m/s.

Figure 4. Two-dimensional autocorrelations of the images of Fig. 3 for a) Sample S1, XY plane, b) Sample S1, ZY plane, c) Sample S2, XY plane, and d) Sample S2, ZY plane. The two graphs on the right of each color map are sections along the white lines in the left images.

Figure 5. Ultrasonic delay fluctuations for (a) Sample S1, and (b) Sample S2. The sound propagates in the Z direction and the transducer is scanned in the XY plane. The color scale is ultrasound delay with an arbitrary zero time offset.

Figure 6. Two-dimensional autocorrelations of the images of Fig. 5 for (a) Sample S1 and (b) Sample S2. The color scale is autocorrelation amplitude in dB where 0 dB corresponds to the maximum of the autocorrelation. The graphs on the right of each color map are sections along the white lines in the left images.

Figure 7. Schematic diagram illustrating how the characteristic decay lengths measured by EBSD in different planes are inter-related.

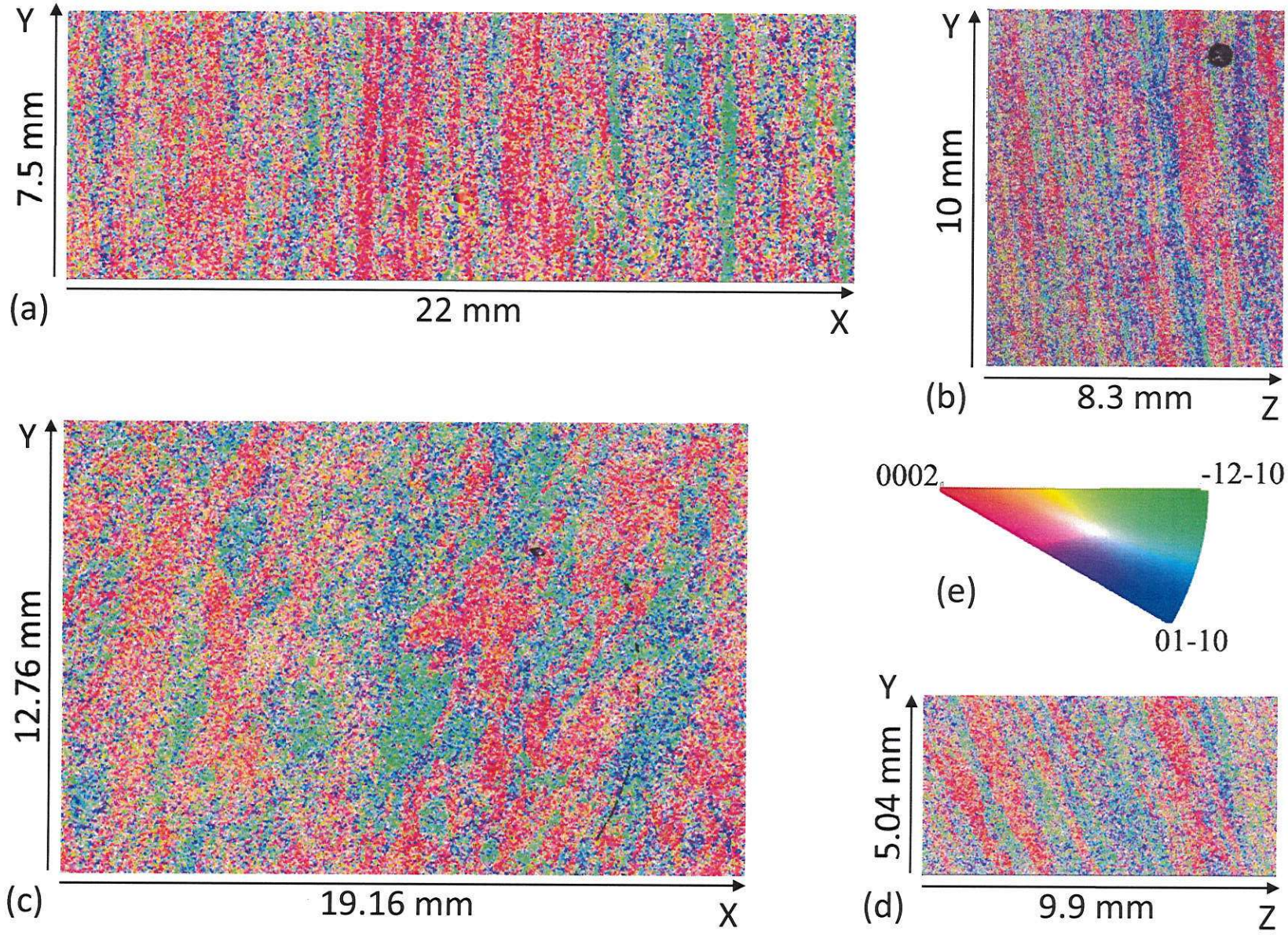
Y
7.5 mm
(a)
22 mm
X
Y
10 mm
(b)
8.3 mm
Z
Y
12.76 mm
(c)
19.16 mm
X
0002
-12-10
(e)
01-10
Y
5.04 mm
(d)
9.9 mm
Z

Figure 1

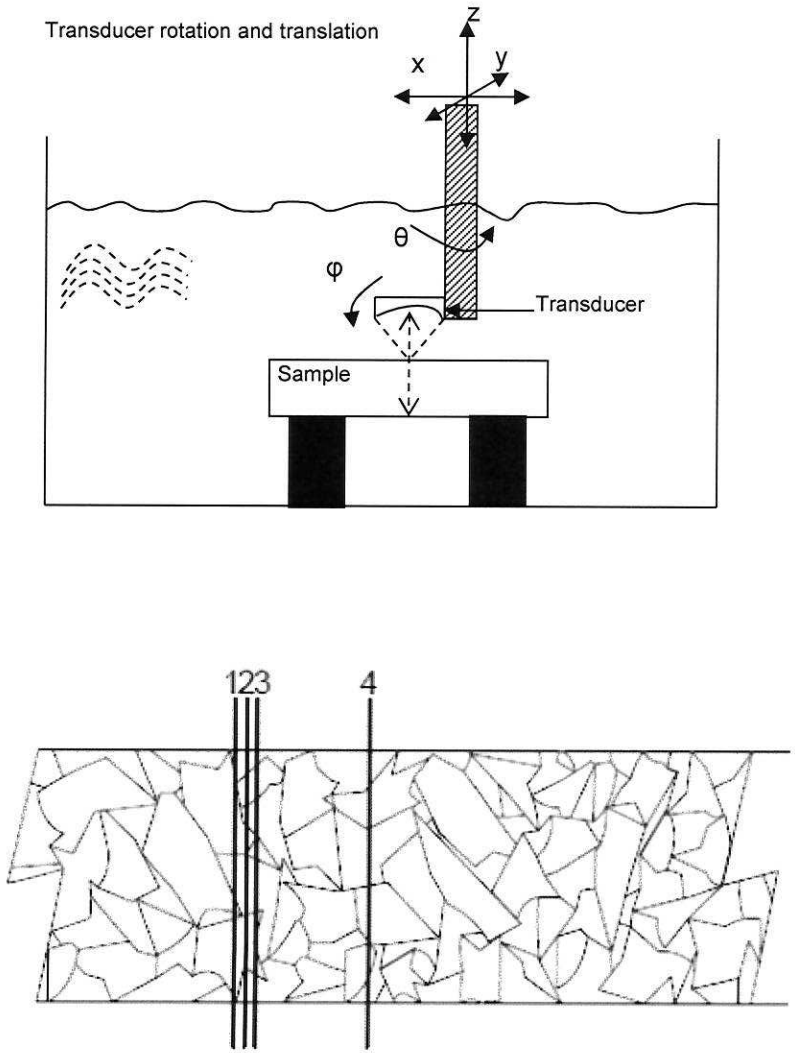
Transducer rotation and translation
z
x
y
θ
φ
Transducer
Sample
123
4

Figure 2

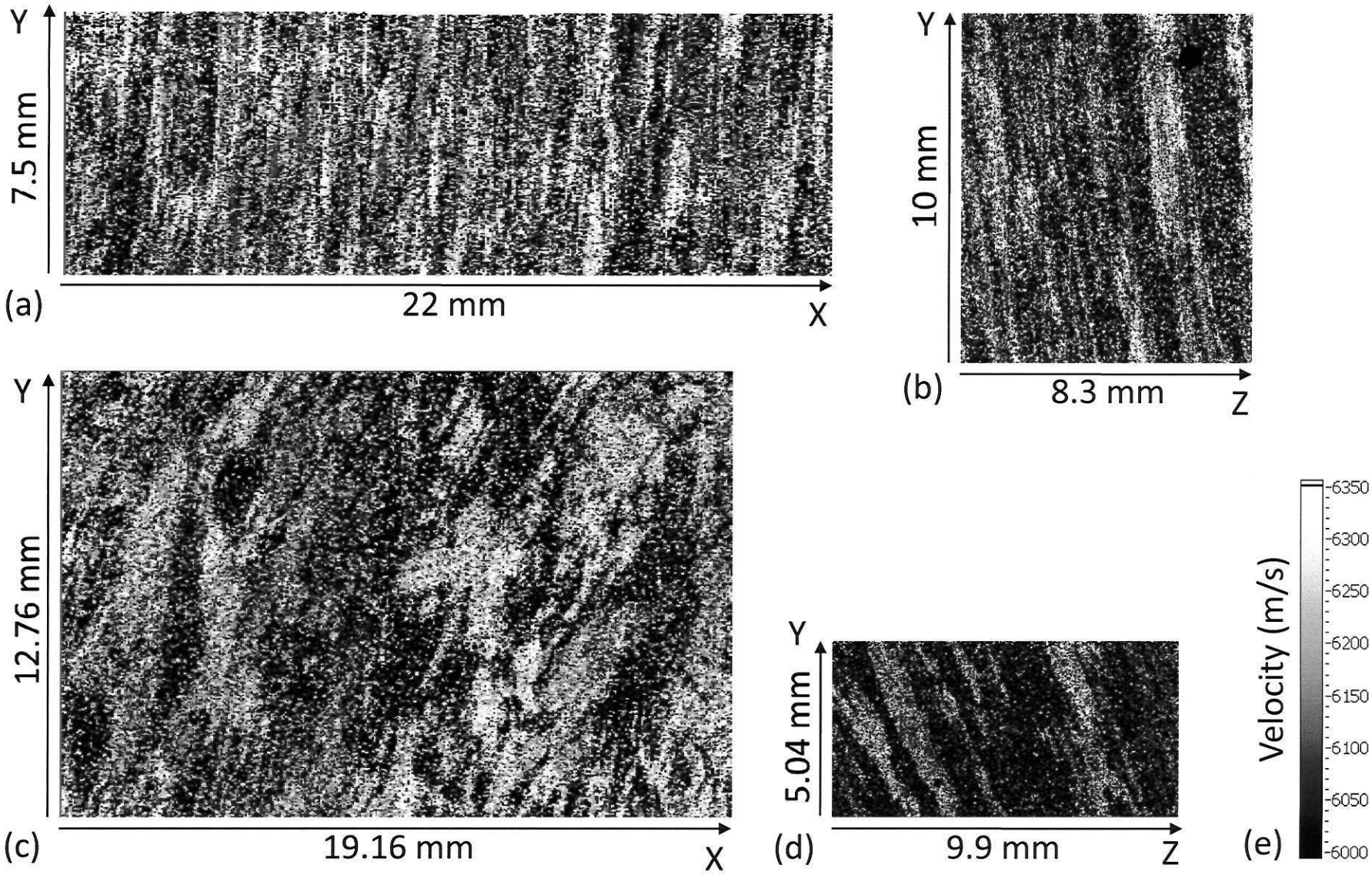
Y
7.5 mm
22 mm
X
(a)
Y
10 mm
8.3 mm
Z
(b)
Y
12.76 mm
19.16 mm
X
(c)
Y
5.04 mm
9.9 mm
Z
(d)
Velocity (m/s)
-6350
-6300
-6250
-6200
-6150
-6100
-6050
-6000
(e)

Figure 3

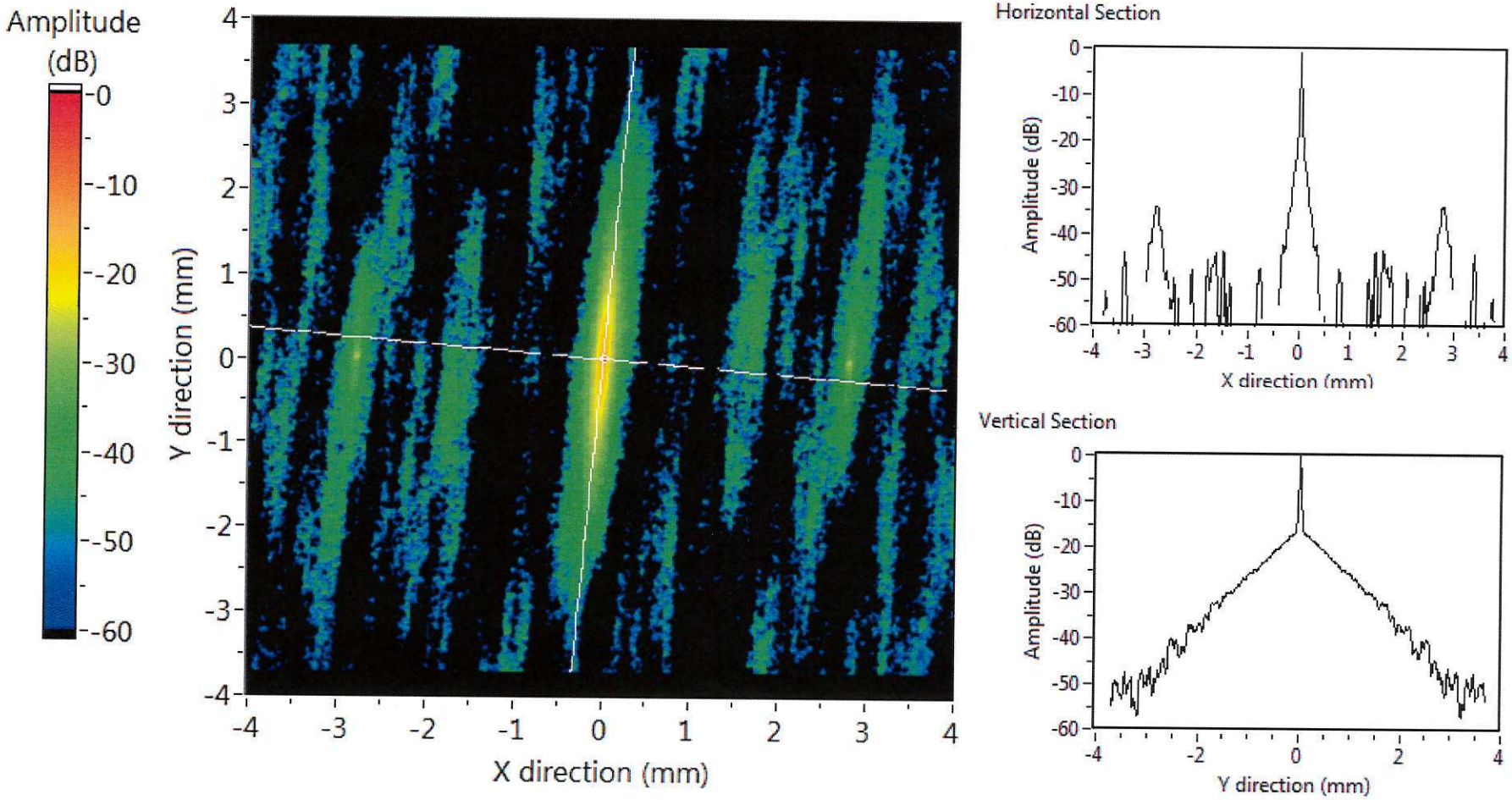
Amplitude
(dB)
-0
--10
--20
--30
--40
--50
--60
Y direction (mm)
X direction (mm)
Horizontal Section
Amplitude (dB)
X direction (mm)
Vertical Section
Amplitude (dB)
Y direction (mm)

Figure 4a

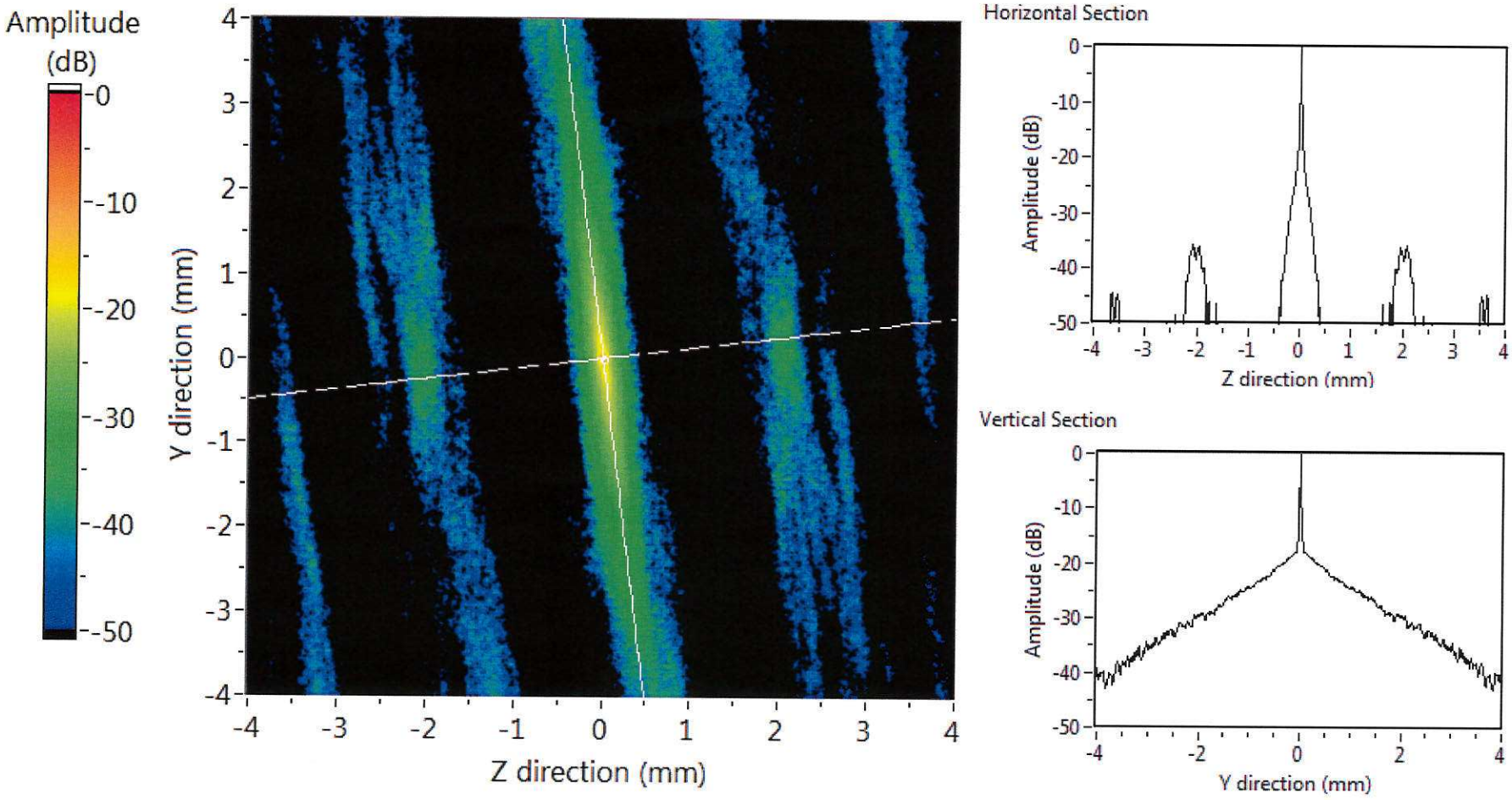
Amplitude
(dB)
-0
--10
--20
--30
--40
--50
Y direction (mm)
Z direction (mm)
Horizontal Section
Amplitude (dB)
Z direction (mm)
Vertical Section
Amplitude (dB)
Y direction (mm)

Figure 4b

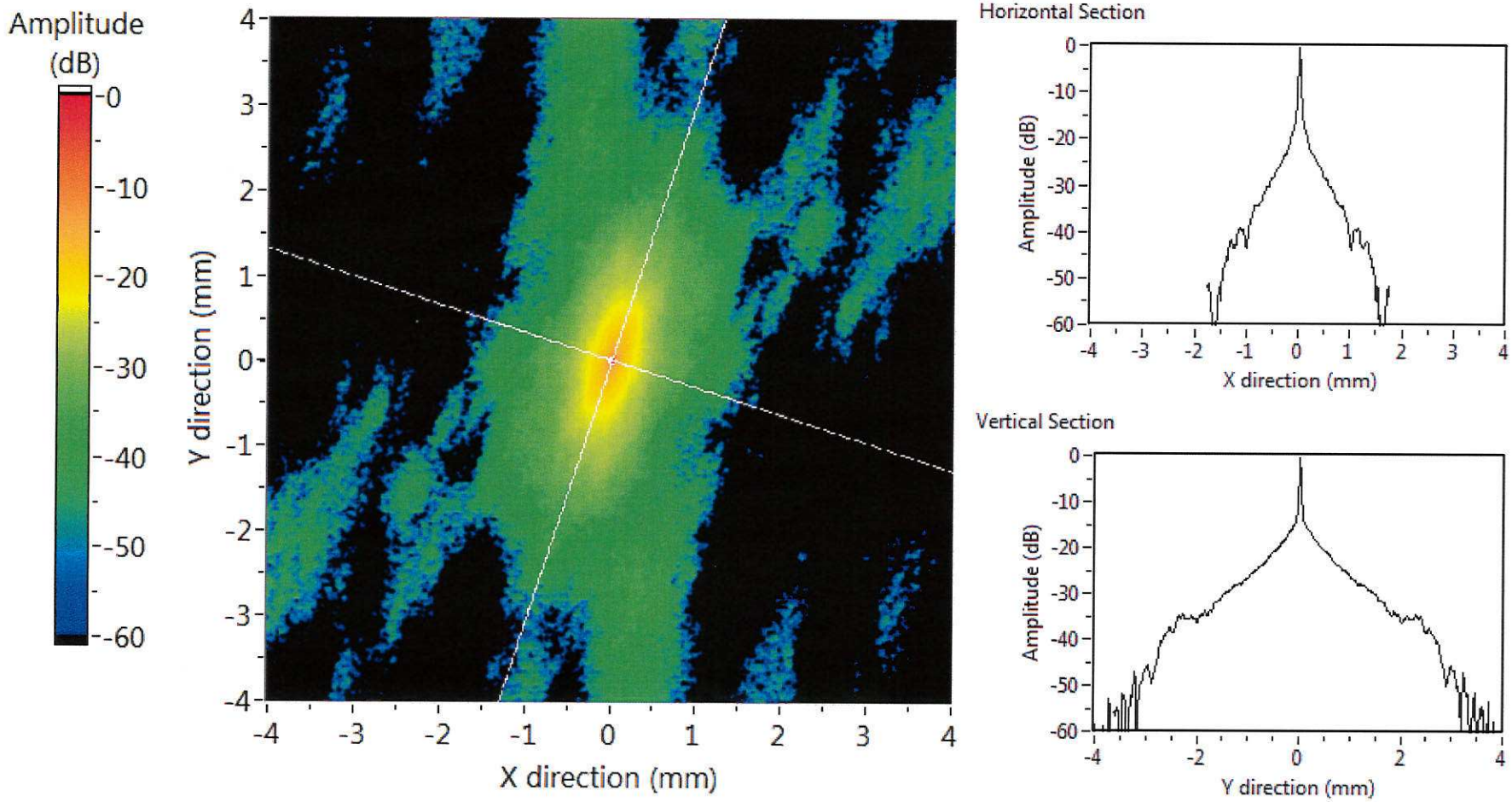
Amplitude
(dB)
-0
--10
--20
--30
--40
--50
--60
Y direction (mm)
X direction (mm)
Horizontal Section
Amplitude (dB)
X direction (mm)
Vertical Section
Amplitude (dB)
Y direction (mm)

Figure 4c

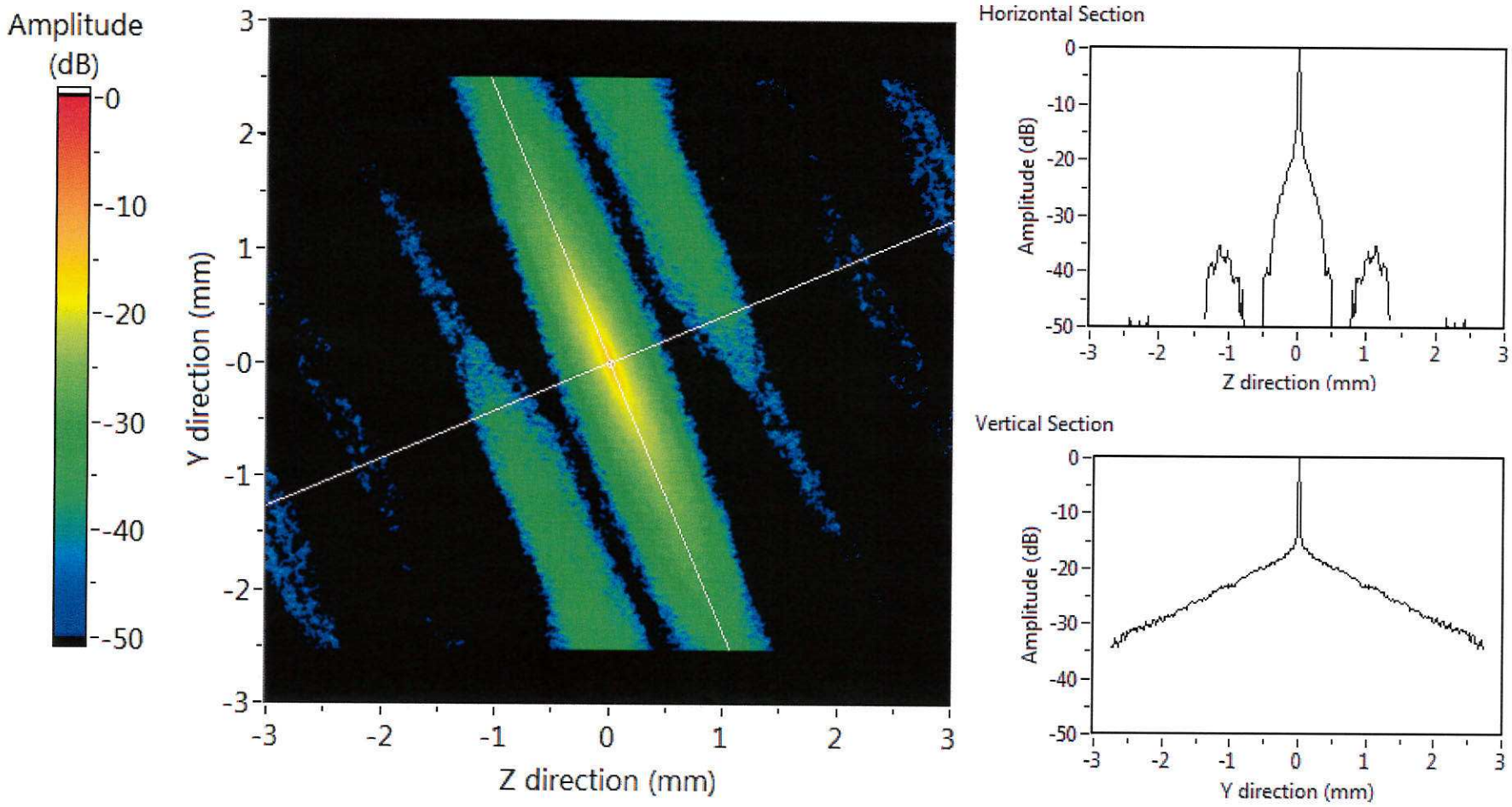
Amplitude
(dB)
-0
--10
--20
--30
--40
--50
Y direction (mm)
Z direction (mm)
Horizontal Section
Amplitude (dB)
Z direction (mm)
Vertical Section
Amplitude (dB)
Y direction (mm)

Figure 4d

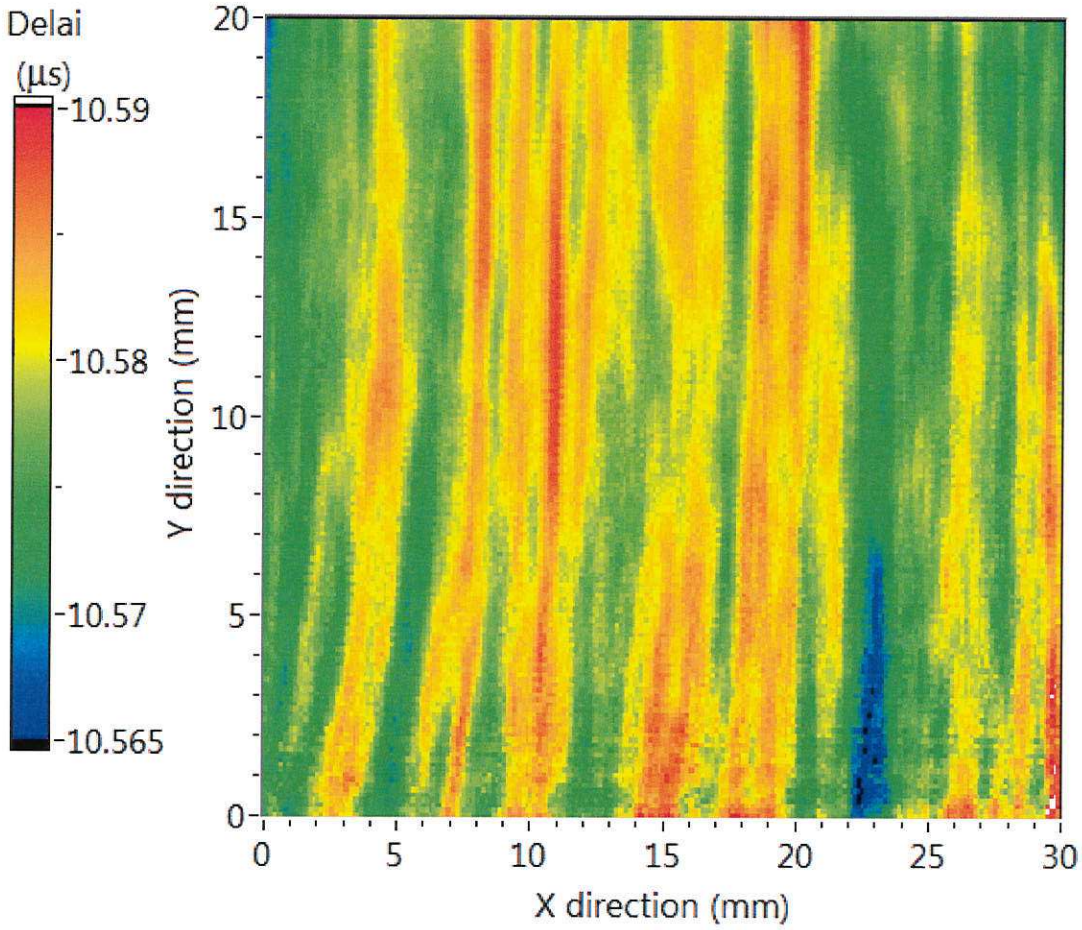
Delai
(µs)
-10.59
-10.58
-10.57
-10.565
Y direction (mm)
0
5
10
15
20
0
5
10
15
20
25
30
X direction (mm)

Figure 5a

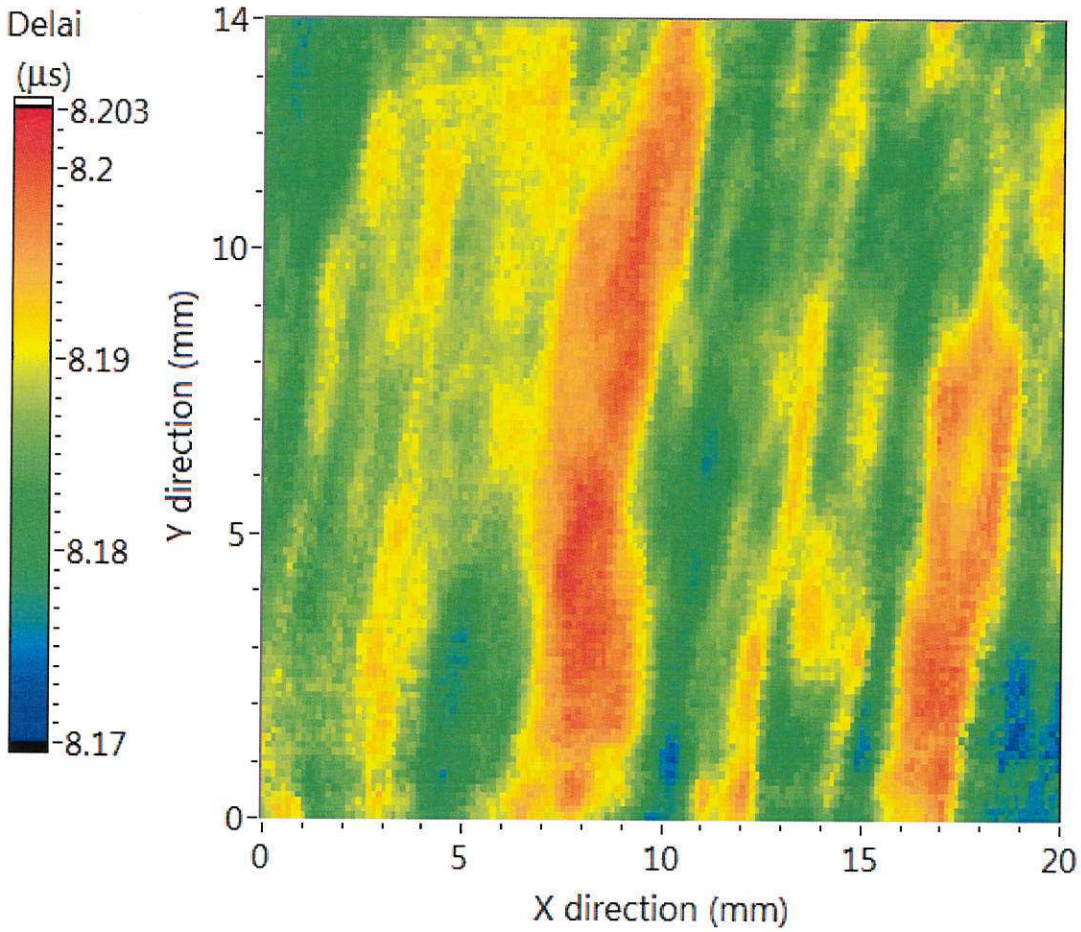
Delai
(µs)
8.203
8.2
8.19
8.18
8.17
14
10
5
0
Y direction (mm)
0
5
10
15
20
X direction (mm)

Figure 5b

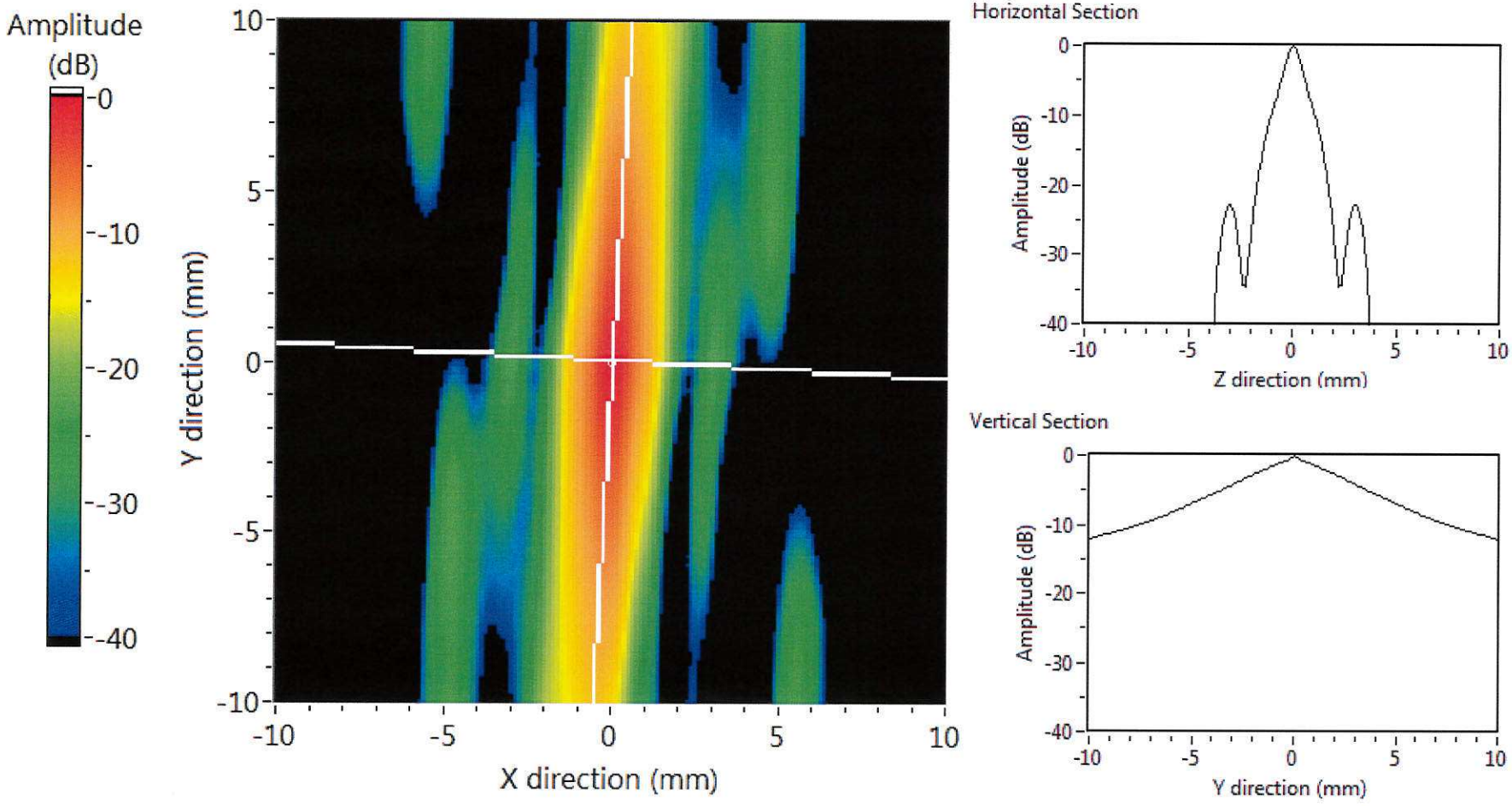
Amplitude
(dB)
-0
--10
--20
--30
--40
Y direction (mm)
X direction (mm)
Horizontal Section
Amplitude (dB)
Z direction (mm)
Vertical Section
Amplitude (dB)
Y direction (mm)

Figure 6a

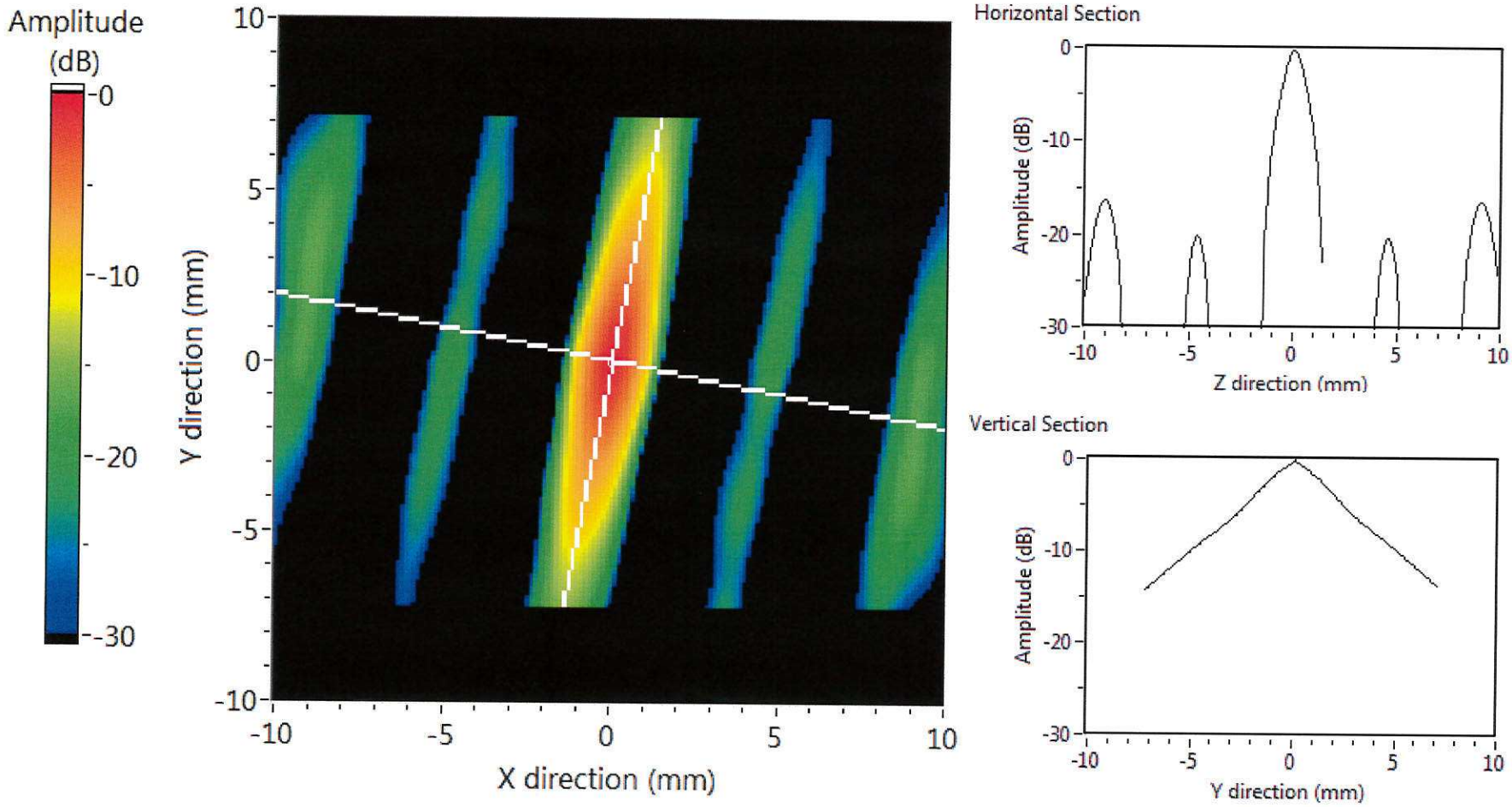
Amplitude
(dB)
-0
--10
--20
--30
10
5
0
-5
-10
Y direction (mm)
-10
-5
0
5
10
X direction (mm)
Horizontal Section
0
-10
-20
-30
Amplitude (dB)
-10
-5
0
5
10
Z direction (mm)
Vertical Section
0
-10
-20
-30
Amplitude (dB)
-10
-5
0
5
10
Y direction (mm)

Figure 6b

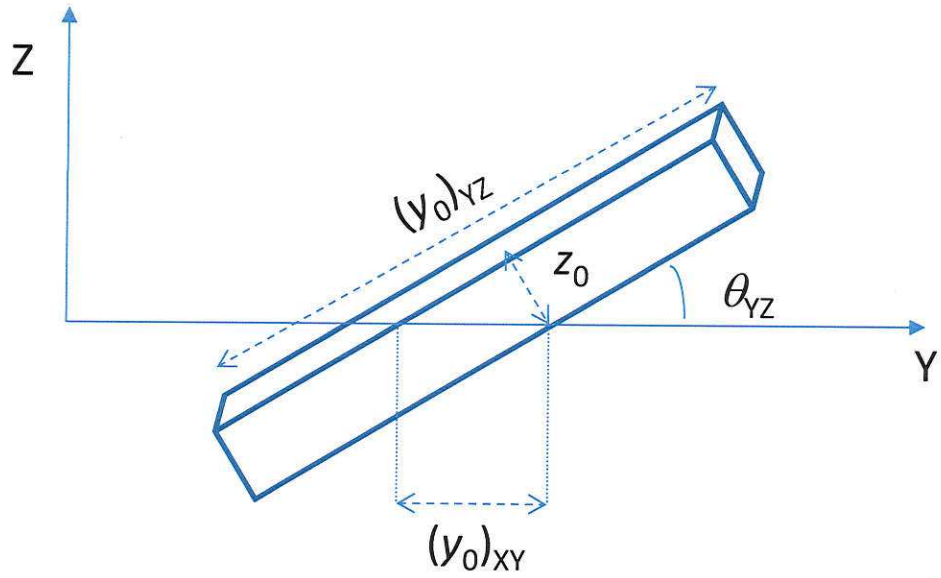

Figure 7